NJC

PAPER

Cite this: *New J. Chem.*, 2018, **42**, 7457

Hybrid bacterial cellulose–pectin films for delivery of bioactive molecules†

Maximiliano L. Cacicedo,[a] Germán A. Islan,[a] M. Florencia Drachemberg,[a] Vera A. Alvarez,[b] Laura C. Bartel,[c] Alejandro D. Bolzán[c] and Guillermo R. Castro*[a]

Received 15th October 2017,
Accepted 26th March 2018

DOI: 10.1039/c7nj03973e

rsc.li/njc

Novel biopolymeric films based on bacterial cellulose (BC) modified with high methoxylated pectin (HMP) were developed for drug delivery. The ability of the films to incorporate an antibiotic, levofloxacin (Levo), was analyzed. Incorporation efficiencies were determined using films with different proportions of HMP (from 0.1% to 2.0%) with a maximum drug payload of 6.23 mg g^{-1}. Characterization studies revealed the existence of a cooperative network between both polymers and deep structural changes in the BC matrix. Besides, the presence of HMP decreased water loss in the BC films from 93% to 75% after 90 min. Additionally, the capacity of the films to incorporate macromolecules was studied using Human Serum Albumin (HSA) as a model protein. The presence of HMP enhanced by more than 3.5 times the encapsulation efficiency (EE) of HSA, and no pH dependence was observed. Release kinetics of both molecules showed hyperbolic profiles with sustained release. In independent experiments, the presence of HMP generated a decrease of around 50% in the release rates of both macromolecules. Additionally, the incorporation of HSA into the BC–HMP matrix modulated the Levo release profile. The antimicrobial activity of Levo released from the BC–HMP–HSA films was confirmed using *Staphylococcus aureus*. *In vitro* studies revealed no apparent cytotoxicity of the released compounds in mammalian CHO cells.

1. Introduction

Globally, wound healing is a challenge clinically and in research because of the social impact triggered by the increasing number of patients with chronic wounds, burns, scalds, and ulcers. According to the World Health Organization (WHO), about 265 000 people die yearly from burns, most of them originating from low- and middle-income countries. In addition, the population in Europe and USA with chronic wounds is in the range of 8.0 to 8.5 million people and accounts for at least 5.5% of the average spending of the health care system.[1,2] Chronic wound cases are increasing worldwide since the population is aging and wounds are associated with illnesses like diabetes and obesity. Diabetes alone affects 422 million people worldwide and consumes between 15% and 25% of the health care resources in medium- and high-income countries (WHO Diabetes Report, 2016). The wounds open the door for pathogens to spread infections in the body. The main therapies involve both systemic and local administration of antibiotics using transdermal patches. However, systemic antibiotic administration may not achieve the desirable antimicrobial concentrations because of the high number of pathogens localized in a wound and the presence of multi-drug resistant microorganisms. Also, increasing antibiotic concentrations can cause undesirable side effects in many organs. Transdermal patches can be useful alternatives since they are easy to manipulate and replace, do not require specific facilities or trained personnel, and can be produced at low cost. Some transdermal patches have been approved by regulatory agencies and are on the market such as anticholinergic, anti-conceptive and nicotine-containing patches. Following this approach, several models for local antibiotic administration have been developed for wound healing therapies including different types of scaffolds prepared from foams, films, hydrogels, *etc.* However, the increase of microbial resistance to common antibiotics has created a global antibiotic emergency as declared by the WHO. A current trend in the market is to combine two antibiotics in a device for local administration. However, this approach can be used for a limited time since antibiotic

[a] *Laboratorio de Nanobiomateriales, CINDEFI, Departamento de Química, Facultad de Ciencias Exactas, Universidad Nacional de La Plata-CONICET (CCT La Plata), Calle 47 y115, C.P. B1900ASH La Plata, Argentina. E-mail: grcastro@gmail.com; Fax: +54 221 483 37 94 ext. 103; Tel: +54 221 483 37 94 ext. 132*

[b] *Grupo de Materiales Compuestos (CoMP), INTEMA (National Research Institute of Material Science and Technology), Facultad de Ingeniería, Universidad Nacional de Mar del Plata, Solís 7575, (B7608FDQ) Mar del Plata, Argentina*

[c] *Laboratorio de Citogenética y Mutagénesis, Instituto Multidisciplinario de Biología Celular (IMBICE, CONICET-CCT La Plata – CICPBA), C.C. 403, 1900 La Plata, Buenos Aires, Argentina*

† Electronic supplementary information (ESI) available: Films photographs, fluorescence quenching analysis, water loss studies. See DOI: 10.1039/c7nj03973e

resistance is growing worldwide. Novel strategies for the development of transdermal patches are exploring the use of alternative molecules, like proteins or peptides for potential therapeutic applications combined with antibiotics. In previous reports, large proteins such as silk fibroin, human recombinant tropoelastin, gelatin and collagen were used to make coacervate scaffolds and improve wound healing.[3–6] Also, fibroblast growth factor was used to regenerate tissue, and keratinases were used for scar debriding in burns, as published elsewhere.[6–8] Following these approaches, the use of therapeutic proteins combined with antibiotics entrapped in transdermal patches could be a useful strategy for wound healing.

Human Serum Albumin (HSA) is a single chain globular protein and the most abundant in human blood plasma, with an extended circulatory half-life. HSA is the natural carrier of many molecules, some of which are hydrophobic (*e.g.* lipids, steroidal hormones among others). It increases their bioavailability by binding them *via* one or more of its three homologous domains (I, II and III). Molecules displaying high affinity to HSA usually bind to sites I and/or II.[9] Because HSA is involved in different metabolic pathways, it is capable of affecting the pharmacokinetics of many drugs, retaining many compounds and protecting them from inactivation, degradation and/or cellular uptake. Different works have considered HSA as an interesting model protein not only as a promising carrier in drug delivery but also as a multi-ligand component able to interact simultaneously with different molecules of therapeutic use (*i.e.* growth factors, anticancer drugs, *etc.*).[10–12]

Levofloxacin (Levo) is an extensively used antibiotic member of the fluoroquinolone family. Levo is an inhibitor of DNA gyrase and topoisomerase IV causing bacterial cell death. Despite their effectiveness, these fluoroquinolone antibiotics are commonly associated with undesirable side effects,[13,14] mainly due to a tendency for aromatic stacking among themselves (*i.e.* π stacking) under physiological conditions, reducing their bioavailability and leading to toxicity.[15] In this sense, the incorporation of fluoroquinolones into biopolymeric devices is a novel technological approach which is potentially useful for providing effective controlled release of the drugs and therefore avoiding toxic concentrations.

Bacterial cellulose (BC) has been intensively studied for many applications in the biomedical field including for artificial blood vessels, tissue engineering, wound dressing, drug delivery, *etc.*[16,17] BC is an extracellular polysaccharide synthesized at the air/culture medium interface of bacterial cultures. BC is produced in nanofibrils composed of β-1→4 glucose units stabilized by inter- and intra-chain hydrogen bonds. In static microbial cultures, the BC nanofibrillar structure is roughly 10 nm thick and 50 nm wide and consists of an extremely pure cellulose network showing high water content (more than 90%), high mechanical strength and well-defined biocompatibility.[18] However, plain BC films do not have antimicrobial activities and neither are they able to entrap, retain and control the release of antibiotics and proteins for therapeutic purposes. Two main strategies have been developed to provide controlled molecular release from the BC films: *ex situ* modification, by the addition of molecules after BC synthesis and purification by chemical or physical methods (*i.e.* chemisorption, covalent derivatization); and *in situ* modification by adding exogenous molecules (*i.e.* polymers) to the culture medium during BC synthesis. Both methods have pros and cons. *Ex situ* methods are more likely to lead to BC surface changes and require extensive purification procedures when chemical modifications are used. Besides, the *ex situ* BC modifications can sometimes be compromised after purification using adsorption procedures. Meanwhile, *in situ* BC modifications allow closer interactions between the cellulose growing fibrils and the exogenous added molecules and form stable molecular films.[5]

Novel biophysical film properties useful for biomedical purposes were found when BC was reinforced by *in situ* modification using alginate.[11,19] BC films have been used for burn treatment, wound healing and antibacterial applications.[16,20–22]

Among biopolymers, pectins have long been considered as matrices for drug incorporation or entrapment and in controlled transdermal or transmucosal drug delivery of active substances.[23] Pectins are water-soluble polysaccharides made of linear residues of mainly poly-alpha-(1,4)-D-galacturonic acid with different esterification degrees (ED), extracted from the plant cell wall. Pectins can be classified as low methoxylated (LMP, below of 40% ED), medium methoxylated (MMP, 40–60% ED), and high methoxylated (HMP, higher than 60% ED). Pectins play a key role in the interactions with antibiotics from the fluoroquinolone family, improving the incorporation of the drug into the matrix and providing a controlled release profile as previously reported.[24]

The aims of the present work were to study and characterize the dual release of a protein model and an antibiotic (*e.g.* HSA and Levo) from BC hybrid membranes containing HMP, for transdermal therapy. Levo and HSA were used as molecular models to study BC–HMP entrapment and kinetic release. The BC films produced by *Komagataeibacter hansenii* (*K. hansenii*) were modified *in situ* by adding different amounts of HMP to the culture. Characterizations of pure BC–HMP films were performed by scanning electronic microscopy (SEM), Fourier transform infrared spectroscopy (FTIR), thermogravimetric analysis (TGA), X-ray diffraction (XRD), and measurements of roughness and water holding capacity. The antimicrobial activities of BC–HMP films loaded with Levo were tested against *Staphyloccocus aureus* (*S. aureus*). The cell viabilities of BC–HMP films were evaluated using CHO cells.

2. Materials & methods

2.1. Chemicals and media

High methoxylated pectin (HMP, 75% methoxylation), levofloxacin (Levo, MW 361.39 Da, (*S*)-9-fluoro-2,3-dihydro-3-methyl-10-(4-methylpiperazin-1-yl)-7-oxo-7*H*-pyrido[1,2,3-*de*]-1,4-benzoxazine-6-carboxylic acid) and Human Serum Albumin (HSA, MW 66 437 Da, isoionic point: 5.2) were provided by Sigma-Aldrich (Buenos Aires, Argentina). All other reagents used were of analytical or

microbiological grade and were purchased from Merck (Darmstadt, Germany).

HSA and Levo were quantified by UV-Vis spectrophotometry (PerkinElmer LS 50B, Japan) at 280 nm and 294 nm, respectively, using appropriate calibration curves.

Cell culture materials were purchased from Corning (Princeton, NJ, USA). Dulbecco's Modified Eagle's Medium (DMEM) and Tryp LE were purchased from Gibco (Gaithersburg, MD, USA), and fetal bovine serum (FBS) was obtained from Internegocios SA (Argentina).

2.2. Bacterial cellulose production with HMP addition

Bacterial cellulose (BC) was synthesized by *Komagataeibacter hansenii* (ATCC 23769) grown statically in the following medium, expressed in g l^{-1}: 25.0 mannitol, 5.0 yeast extract and 3.0 peptone. HMP was added at concentrations of 0.1, 0.5, 1.0 and 2.0%. The pH of the medium was adjusted to 6.5 with 100 mM NaOH solution before sterilization. The cultures were maintained statically in 96-well plates at 27 °C for 14 days.

2.3. Bacterial cellulose purification

Native cellulose and hybrid cellulose films were collected from the plates for the purification process and washed three times with a 70% ethanol solution for 60 minutes. Later, the purification was performed using 70% ethanol/0.1 N NaOH solution for 24 h at 30 °C. After that, repetitive washes with 70% ethanol were performed until the pH was neutral. Finally, the films were exposed to a solution of 70% ethanol/500 mM $CaCl_2$.

2.4. Levo loading studies

BC systems were dipped in 1.0 and 5.0 mg ml^{-1} Levo aqueous solutions and stirred at 230 rpm at 25 °C for 20 h. The membranes were then taken out from the vials and the remaining Levo was spectrophotometrically assayed in the supernatants.[19] Membranes were washed once in 80% ethanol and later in physiological solution for 10 minutes. The loading efficiency was evaluated as follows:

$$\text{Levo incorporation} = \frac{(\text{LevoI} - \text{LevoS})}{\text{WBC}}$$

where LevoI and LevoS are the mass (mg) of Levo in the supernatant at time zero, and after 20 h incubation respectively, and WBC is the mass of BC film (grams).

Control assays without membranes were performed. Neither Levo degradation, nor a shift in the UV maximum nor a decrease in intensity was observed after antibiotic incorporation into the matrix.

2.5. BC–HMP film characterization

2.5.1. Scanning electron microscopy (SEM). Samples were firstly dried using the critical point technique. After that, sputtering was performed on the surface with gold using a metalizer (Balzers SCD 030) to obtain a layer thickness of between 15 and 20 nm. Film surfaces and morphologies were observed by SEM (Philips SEM 505 model, Rochester, NY, USA), and the images were processed using a digitizer program (Soft Imaging System ADDA II).

2.5.2. Roughness analysis. SEM images were analyzed by ImageJ software (NIH, USA). Differences in surface parameters (roughness, polymer distribution) were reflected by the mean and standard variation of the gray values of all the pixels on the images.[25] Histograms were constructed from duplicates of SEM images at 1000× magnification. The plot profiles were obtained from images at 5000×.

2.5.3. Vibrational spectroscopic analysis (FTIR). Free Levo, HMP and HMP–Levo mixtures were analyzed by FTIR (JASCO FT/IR-4200). Pellets were prepared by mixing the samples at 5.0% (w/w) with potassium bromide (Pike Technologies) and with a background correction of 256 scans, against a high-energy ceramic source and DLATGS detector.

Additionally, FTIR spectra of the lyophilized BC samples were recorded in a spectrometer (Thermo Scientific Nicolet, model 6700, CT, USA) coupled to an ATR (attenuated total reflectance) accessory for all measurements. Each sample was scanned 32 times in the 600 cm^{-1} to 4000 cm^{-1} range with a resolution of 4 cm^{-1}.

2.5.4. Thermogravimetric analysis (TGA). Dynamic thermogravimetric measurements of native and hybrid BC membranes were performed using a Shimadzu TGA-50 instrument. Tests were run in the range of 20 °C to 900 °C with a heating rate of 10 °C min^{-1} under an N_2 atmosphere. TGA assays displayed less than 1% differences between sample values.

2.5.5. X-ray diffraction (XRD). XRD patterns of cellulose film samples were collected in reflection mode on a glass substrate. The measurements were performed with an Analytical Expert instrument using Cu-Kα radiation (λ = 1.54 Å) from $2\theta = 10^\circ$ to 70° in continuous mode with a step size of 0.07°. The results were analyzed using Origin software.

2.5.6. Porosimetry. Mercury intrusion porosimetry (MIP) was performed using a pressure of up to 200 MPa (Pascal-Thermo Fisher 440 and 140). The assumptions were: 4.65×10^{-5} N m^{-1} mercury surface tension, 13 534 kg m^{-3} mercury density and an advancing/receding contact angle of 130°. The amount of mercury intruded at each pressure interval was recorded. Film samples of 1 cm in diameter were freeze dried and stored in an air-tight receptacle prior to evaluation.

2.5.7. Water holding capacity (WHC) studies. BC and BC–HMP films were incubated at 37 °C in a culture incubator. The films were weighed in an analytical balance every 30 minutes for 2 h.

2.6. HSA loading studies

HSA incorporation efficiency was evaluated in BC hybrid films containing 2.0% HMP. BC films were used as a control. Films were immersed in 5.0 mg ml^{-1} HSA solutions in 200 mM buffers at pH 5.5 (acetate), 7.0 (phosphate) and 9.0 (Tris). The HSA loading efficiencies were evaluated using a procedure similar to that used for Levo loading.

2.7. *In vitro* drug release studies

BC membranes were placed in 1.5 ml acetate buffer (pH 5.5) in 2.0 ml plastic vials at 37 °C. Samples of 500 μl were withdrawn and replaced with equal volumes of fresh buffer at defined intervals.

Levo and HSA concentrations in the samples were spectrophotometrically determined as mentioned before. Kinetic release experiments were performed twice in quadruplicate.

2.8. Fluorescence quenching studies

Levo binding to HSA was evaluated from the quenching of HSA auto fluorescence using a method modified from a previous report.[21] HSA solutions at 1.0 mg ml^{-1} were subjected to the addition of Levo solutions in the range 11.0–275.0 μM. In order to stimulate molecule binding, the mixtures were incubated at 37 °C for 20 minutes with agitation. Fluorescence spectra were recorded in the range 300–400 nm after excitation at 295 nm and the intrinsic fluorescence emission of protein was monitored at 350 nm. It is relevant to mention that the intrinsic fluorescence from Levo did not interfere with the analysis, since its emission occurred at around 470 nm.

2.9. Antimicrobial studies

Levo activity was tested against *Staphylococcus aureus* using a modified disk diffusion method, replacing disks with films. Briefly, bacteria were grown in nutrient broth up to 10^8 UFC per ml at 37 °C for 24 h until they reached the exponential phase. They were then spread over Mueller–Hinton agar plates. BC–HMP films loaded with Levo and HSA were placed on the surface of the plates and incubated at 37 °C for 24 h. Levo and Levo + HSA solutions of the same concentration as those in the films were used as controls. Each solution (25 μl) was placed inside a sterile glass cylinder and incubated at 37 °C for 24 h.[24] Later, inhibition haloes in the plates were determined.

2.10. Cytotoxicity assays

The cytotoxicity of Levo in the presence of HMP was tested in CHO-K1 cells using the MTT (3-(4,5-dimethylthiazol-2-yl)-2,5-diphenyltetrazolium bromide) assay, which is based on the ability of living, metabolically active cells to cleave a tetrazolium salt.[26] The CHO-K1 cell line was obtained from the IMBICE cell repository, and was selected as the *in vitro* model due to its wide use for *in vitro* toxicity studies and the uniform properties it exhibits. CHO cells were grown in Ham's F10 medium supplemented with 10% FBS, penicillin (100 U ml^{-1}) and streptomycin (100 mg ml^{-1}) in a 5% CO_2 atmosphere at 37 °C. They were seeded on 96-well plates at a density of 10^4 cells per well and allowed to adhere for 24 h. Then, cells were exposed to: the biopolymer (HMP, 2.0%, p/v), free Levo (at 50, 100 and 200 μg ml^{-1}) or Levo in the presence of HMP for 24 h. Once the incubation time was completed, the medium was carefully discarded and a volume of 100 μl of MTT solution (0.5 mg ml^{-1} in medium without FBS and phenol red) was added to each well. The presence of violet crystals inside the cells was monitored by optical microscopy after 3 h of incubation. The contents of the wells were discarded, wells were carefully washed with PBS and 100 μl of DMSO was added to each well to extract formazan crystals. The absorbance at 550 nm was measured at room temperature after a short incubation time. The assay was performed in four independent experiments each in sextuplicate.

2.11. Statistical analysis

All experiments were carried out three times with a minimum of three replicates each. According to the number of groups to be compared, comparisons of the means were performed by Student *t*-test or by analysis of variance (ANOVA, followed by Tukey's HSD test). A significance level of 0.05 was used.

3. Results & discussion

3.1. Levo loading studies in modified BC films

BC films containing pectin (BC–HMP) were evaluated for the incorporation of Levo. The incorporation efficiency of 1.0 mg ml^{-1} Levo was around 0.4 ± 0.1 mg per g of matrix in BC films containing 0.0 to 1.0% HMP ($p \geq 0.05$, data not shown).

However, the drug payload was raised about 10 fold when the Levo concentration of the immersion solution was increased to 5.0 mg ml^{-1} (Fig. 1). Also, a significant increase in Levo incorporation efficiency of 50% ($p \leq 0.05$) was shown when BC films were produced in a culture medium supplemented with 2.0% HMP. A possible BC structural modification induced by the presence of HMP could allow residual hydrophobic groups to be exposed that could interact non-covalently with the aromatic ring of Levo resulting in an increase of drug incorporation.

3.2. BC–HMP film characterization

Drug incorporation experiments showed that the BC film supplemented with 2.0% HMP might have potential biomedical applications. Next, characterization analyses of the hybrid matrix were performed to understand how the BC network was modified by the presence of HMP. Significant color and texture differences were observed by the naked eye between BC and BC–HMP (Fig. S1, ESI†). Consistent with this, SEM images of both films confirmed the differences between them and showed the presence of gel structures composed of interconnected fibers (Fig. 2).

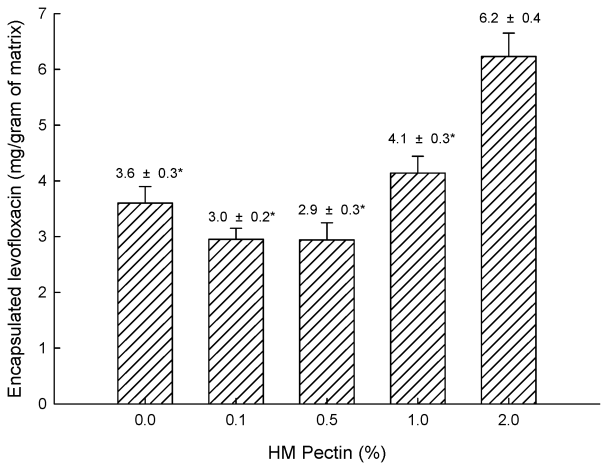

Fig. 1 Effect of HMP content on Levo incorporation in hybrid BC–HMP films. The Levo concentration of the immersion solution was 5.0 mg ml^{-1}. Results are expressed as the mean of two independent experiments, each performed in triplicate. Note: * indicates that no significant difference was found ($p \geq 0.05$).

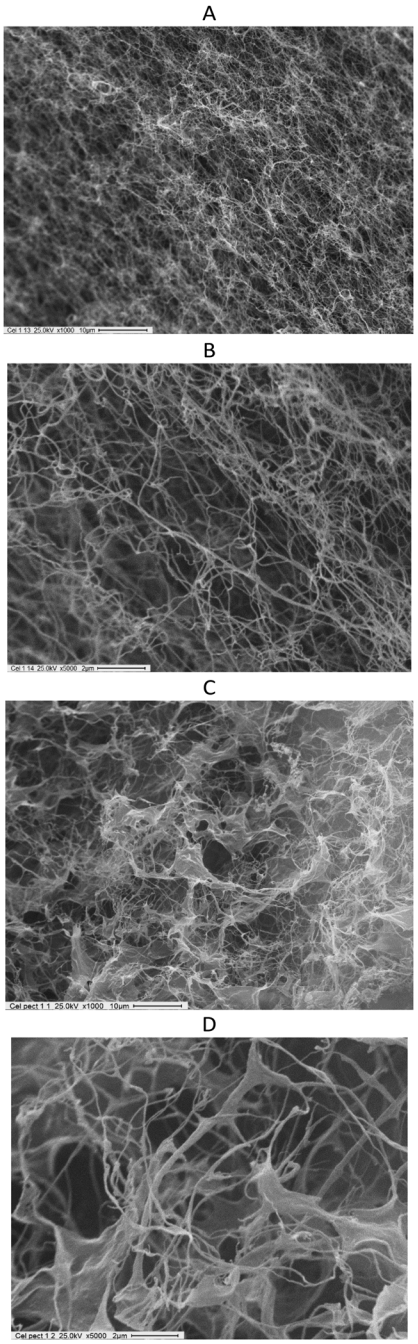

Fig. 2 SEM images of BC (A and B) and BC–HMP films (C and D) at 1000× and 5000× magnifications, respectively.

As previously reported, long cellulose nanofibrils were three-dimensionally disposed to produce stable structured films (Fig. 2A and B). When HMP was incorporated into the BC network, a hybrid nanocomposite was produced with cooperation between both biopolymers. A thickening of cellulose fibers was clearly observed by SEM, showing the modification of the initial cellulose films (Fig. 2C and D). Similar results were previously reported for BC–alginate composites.[19] *In silico* surface analysis of the BC and BC–HMP films was carried out to determine semi-quantitative differences (Fig. S2, ESI†). The change of the mean value of the standard deviation in BC–HMP films indicates modifications in the spatial structure alignment of the biopolymeric chains.

Also, the increase in the standard deviation of the BC–HMP hybrid film can be correlated with the presence of a rougher surface due to the incorporation of HMP into the BC film.[27] This result was also observed in the modification of the histogram after HMP incorporation into the BC film (Fig. 1), certainly due to the formation of an entwined network between both biopolymers with similar structural and chemical characteristics.[19] The plot profile of the BC film displayed the presence of nanofibers, which were distributed in a narrow diameter range with a mean of 79.5 ± 9.7 nm. An increase in those values was observed after incorporation of pectin, with diameters ranging from 200 nm to 500 nm and an average mean of 322.7 ± 98.0 nm, which suggests the interpenetration of HMP into the cellulose matrix. The thermal properties of native BC, HMP and BC–HMP films were investigated by TGA. The tests were carried out in a nitrogen atmosphere to avoid thermo-oxidative processes. Two step decomposition curves were observed for unmodified bacterial cellulose and HMP (Fig. 3).

Meanwhile, the weight loss profile for BC–HMP showed a curve with three main steps. The first step was attributed to unbound water, observed in the temperature range between 30 °C and 120 °C. At 200 °C the percentage of weight loss was around 8% for BC, 15% for HMP and 20% for BC–HMP. The results showed that there was a higher water content in the hybrid matrix as compared to the BC membrane because of the high water content of HMP. It is generally accepted that water acts as plasticizer in hydroxylic polymeric matrices.[28]

The second step on Fig. 3 was attributed to the thermal degradation of biomaterial. Analyses were performed on the thermal degradation curves and relevant differences were observed between native BC and modified BC (Table 1).

The biggest weight losses in the range of 200 °C to 400 °C were 68.5% and 30.4% for BC and BC–HMP respectively. The increased thermal stability of BC–HMP films could be associated with the high interpenetration of the BC and HMP polymer chains.[19]

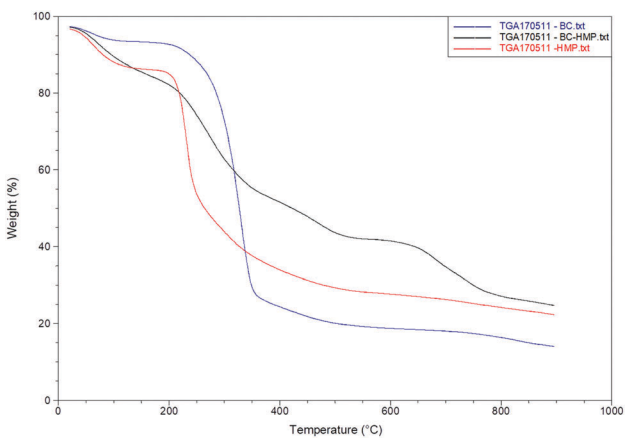

Fig. 3 Thermogravimetric curves for BC, HMP and BC–HMP films.

Table 1 Relevant values from thermal degradation analysis of BC, BC–HMP and HMP

Parameter	Films		
	Cellulose	HMP	BC–HMP
Mass loss (200–400 °C, %)	68.5	51.4	30.4
T_{50} (°C)	326.9	264.4	423.0
Residue at 750 °C (%)	17.5	25.2	29.9

Additionally, a significant change in the 50% weight loss temperature (T_{50}) was found in the hybrid film. BC–HMP exhibited an increased decomposition temperature from 326.9 °C (native BC) to 423.0 °C. Furthermore, BC–HMP showed almost 50% more residual mass than BC at 750 °C. The three evaluated parameters confirm the integration of HMP into the polymeric network of BC.

FTIR analyses were performed to determine the interaction characteristics of the film components observed in the TGA experiments (Fig. 4). The BC film showed peaks centered at 3346 cm^{-1} and 2894 cm^{-1}, assigned to ν_{O-H} and ν_{C-H} bands respectively. Also, a peak centered at 1060 cm^{-1} was assigned to C–O stretching, in agreement with a previous report.[29] HMP was characterized by the presence of stretching carbonyl bands of the free acid (ν_{COOH} = 1733 cm^{-1}) and the esterified carboxyl groups (ν_{COOCH_3} = 1604 cm^{-1}).[30] FTIR spectra of BC–HMP showed several changes compared to the BC and HMP profiles. The peak corresponding to C–O stretching decreased considerably in its intensity and shifted to 1097 cm^{-1}.

This result suggests that the hydrogen bonding patterns inside the polymeric network might be changing because of a shift from an ordered 3D-structure to a more disordered one.[31] Also, the characteristic peaks of the HMP carboxylic residues (1733 cm^{-1} and 1604 cm^{-1}) shifted and overlapped at 1600 cm^{-1}. These changes can only be attributed to the interactions between HMP and BC. Finally, the bands in the region from 3000 cm^{-1} to 3600 cm^{-1} commonly assigned to O–H stretching and used to elucidate hydrogen bonding patterns became much broader after the BC modification with HMP, suggesting that inter-molecular hydrogen bonds are playing a weaker role in the hybrid BC–HMP polymeric network.[32]

The disruption of hydrogen bonds by HMP could be responsible for interference in cellulose crystal synthesis, increasing the amorphous phase of the biomaterial.[31,33] Also, the reduction of hydrogen bonds could leave more free –OH groups exposed both in the interior and on the surface of the matrix.[32] The increase in the amorphous phase and free –OH groups of the BC matrix could enhance the interaction of molecules with the components of the polymeric matrix. These results agree with the experimental observations displayed in the incorporation experiments (Fig. 1). In addition, FTIR spectra of HMP, Levo and the blend of both were obtained to investigate possible interactions between Levo and the biopolymer (Fig. 5). The Levo main vibrational bands were associated with carbonyl ($\nu_{C=O}$ = 1730 cm^{-1}), amine (ν_{C-N} = 1295 cm^{-1}) and fluorine (ν_{C-F} = 1078 cm^{-1}) groups.[34] HMP was mainly characterized by the presence of bands of free (ν_{COOCH_3} = 1604 cm^{-1}) and esterified (ν_{COOH} = 1733 cm^{-1}) carboxyl groups.[30]

FTIR spectra of HMP–Levo showed changes in these typical vibrational bands. A blue shift of 13 cm^{-1} was observed for the band of the free carboxyl group, and a red shift of 21 cm^{-1} was seen for the methoxylated groups. Additionally, a new band at 1271 cm^{-1} assigned to C–N stretching was observed.

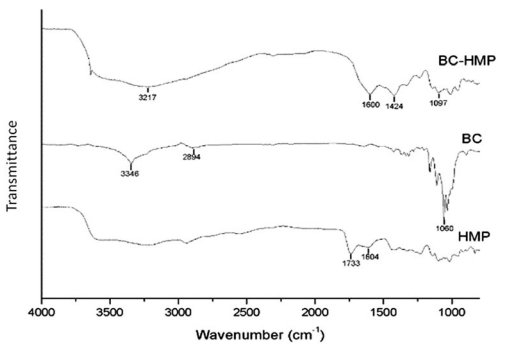

Fig. 4 FTIR spectra of BC, HMP and BC–HMP.

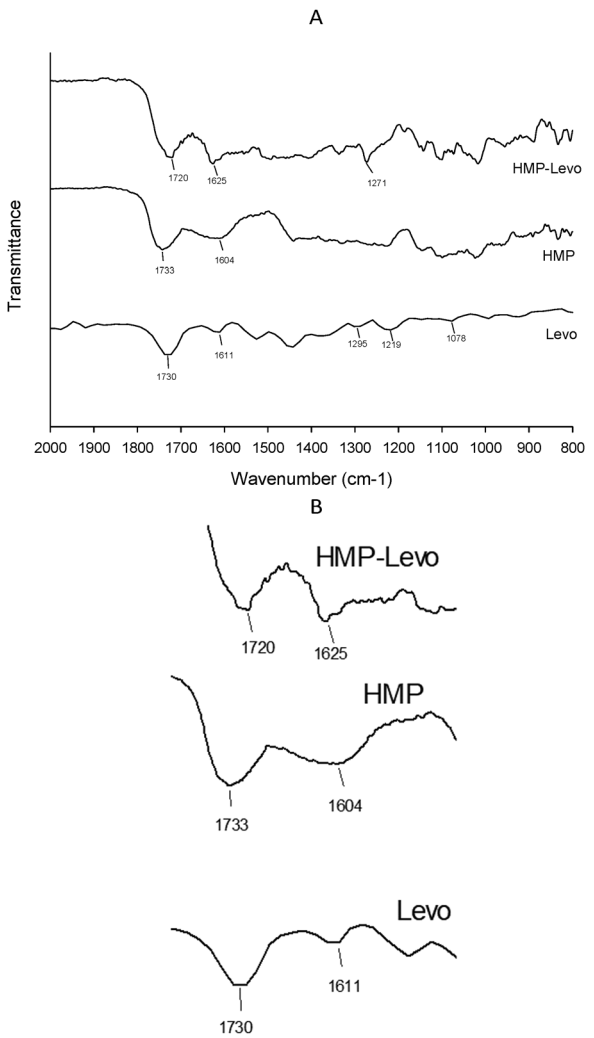

Fig. 5 (A) FTIR spectra of Levo, HMP and the blend of both components. (B) Amplification of FTIR spectra in the range 1500–1800 cm^{-1}.

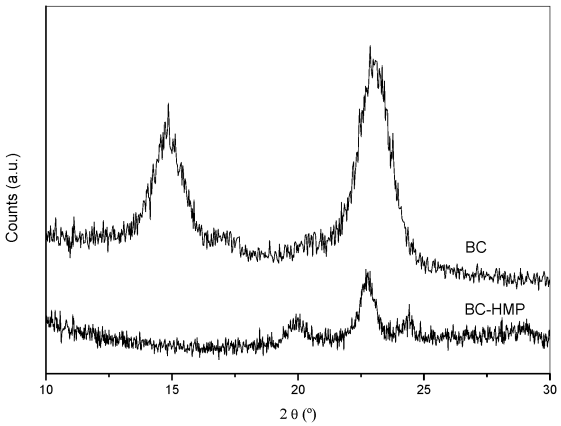

Fig. 6 XRD spectra for BC and BC–HMP scaffolds. HMP was also assayed as a control.

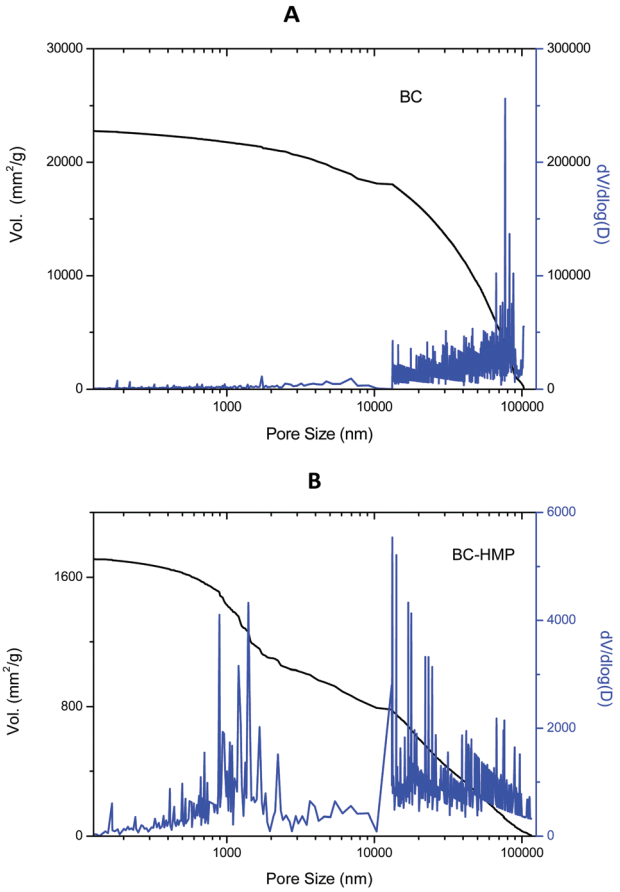

Fig. 7 Cumulative MIP and pore size distributions of the BC (A) and BC–HMP composite (B).

These results suggest that there is a strong interaction between the HMP and Levo, in agreement with previous reports showing polar and non-polar interactions between pectins and fluoroquinolones (*i.e.* enrofloxacin and ciprofloxacin).[35,36]

Furthermore, the structural changes generated on BC films by the addition of HMP were analyzed by XRD (Fig. 6). The XRD profiles of BC showed characteristic Bragg's angles of $2\theta = 14.6^{\circ}$, 16.9° and 22.8° which were indexed as the (1 1 0), (0 1 0) and (0 0 2) reflection planes respectively. Besides HMP did not shown any peaks because of its amorphous nature (Fig. S5, ESI†). Meanwhile, BC–HMP exhibited a strong reduction in the (0 0 2) peak and the disappearance of the (1 1 0) and (0 1 0) peaks; these changes indicate a significant structural change in the polymeric network. Besides, a peak in the region corresponding to the amorphous phase ($2\theta = 18^{\circ}$–20°) was noticed in BC–HMP.[32,37] Based on these results, the crystallinity index was calculated by Segal's method[37] using the following equation:

$$\mathrm{CI} = \frac{100[I(002) - I_{\mathrm{am}}]}{I(002)}$$

where I(0 0 2) is the peak intensity of the (0 0 2) peak for cellulose I, and I_{am} is the intensity diffraction of the amorphous fraction at the minimum between the (1 1 0) and (0 0 2) peaks.

A significant decrease in the crystallinity index from 68.9% for BC to 46.9% for BC–HMP was observed. Several reports have reported some decrease in BC crystallinity after *in situ* and *ex situ* modifications with different kinds of molecules like alginate, poly(ethylene glycol), graphene, hydroxypropylmethyl cellulose, carboxymethyl cellulose and xyloglucan.[19,32,38–40] A decrease in the crystallinity index is generally related to an increment in the amorphous phase of the matrix, concomitant with an increased water absorption capacity. These results confirm the assumptions drawn from the FTIR analysis where it was suggested that the presence of HMP partially interferes with the self-assembly of BC fibers and therefore strongly reduces the cellulose crystalline structure.

The macroporous and mesoporous volumes and the pore size distribution for the BC and BC–HMP samples were analyzed by MIP (Fig. 7). According to the graphs in Fig. 7, the contribution of the mesoporous volumes of both materials is negligible. The BC sample has a more homogeneous pore size distribution, approximately in the range 10 000 nm to 100 000 nm (Fig. 7A). Meanwhile, the BC–HMP scaffold has a wider pore size distribution than the BC sample, displaying two main regions: one between 100 and 10 000 nm and a second region between 10 000 and 100 000 nm (Fig. 7B). The results of FTIR and XRD, which showed an increase in the amorphous structure of BC after the addition of HMP to the films, could be reflected in an increase in water interactions within the hybrid matrix since more free hydroxyl residues would be able to establish hydrogen bonds with the surrounding water. Moreover, an analysis of water loss in BC films was tested by weight changes in an open atmosphere at 37 °C (Fig. S3, ESI†). The kinetic results of water loss in BC showed a fast decay with less than 25% of the water content remaining after 30 min and a stable residue of about 7% after 90 min. Meanwhile, the BC–HMP displayed about 40% water content at 30 min and stability after 90 min with about 25% water content. The results indicate that the addition of HMP to the BC film produces a considerable increase in water retention by the hybrid matrix associated with the inter-molecular hydrogen bridges within the aqueous media. Moreover, the results reveal that BC–HMP films have more total water content (84.6 ± 8.4 mg per film) than unmodified BC (63.3 ± 6.9 mg per film) ($p \leq 0.05$).

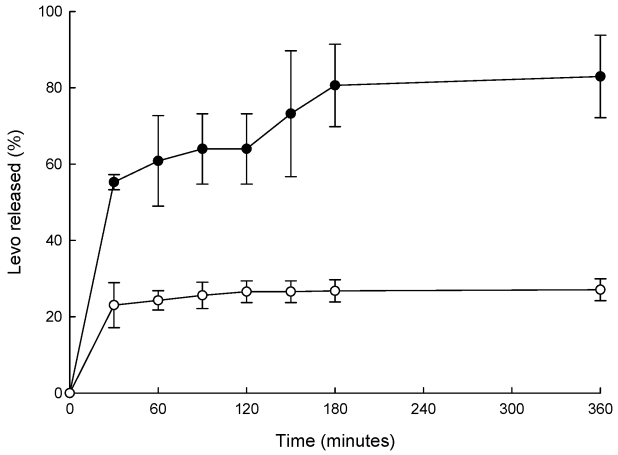

Fig. 8 Kinetic release profiles of Levo from BC (–●–) and BC–HMP (–○–) films, performed at pH 5.5 and 37 °C.

3.3. Levo kinetic release assays

Kinetic release experiments of Levo from BC and BC–HMP films showed hyperbolic curves (Fig. 8). The presence of HMP in the BC films reduced the release of the cargo molecule.

In particular, only 27% of the loaded Levo was released from BC–HMP films after 6 h. Meanwhile, 83% Levo was released from BC films at the end-point of the assay. These kinetic release experiments indicate that the presence of HMP enhances the suitability of the BC film for sustained drug release applications.

3.4. Cytotoxicity studies

The cytotoxicity of BC systems has been carefully studied by different methods, demonstrating that bacterial cellulose fibers do not produce *in vitro* toxic effects on mammalian cells.[41]

However, the present system contemplated the incorporation of two new components into the matrix: the antibiotic and HMP. Considering that those two molecules could diffuse away from the cellulose matrix, their cytotoxicity was evaluated against CHO-K1 cells as a model system (Table 2). Levo was tested at concentrations ranging from 0 up to 200 μg ml^{-1}, in consideration of the therapeutic serum concentrations.[42] As previously reported, Levo produced a cell viability decrease in a concentration-dependent manner with 11% and 29% reduction for 100 and 200 μg ml^{-1} of Levo respectively.[24]

Table 2 Cytotoxicity assay of Levo in the presence of HMP, tested in CHO-K1 cells by the MTT method

	Cell viability[a] (%)		
	Quinolone concentration (μg ml^{-1})		
	50	100	200
Control (untreated)	100.0 ± 8.1^{1}		
HMP	95.5 ± 12.3^{1}		
Levo	97.5 ± 10.8^{a,1}	89.2 ± 19.8^{a,2}	71.3 ± 9.3^{2}
HMP–Levo	103.8 ± 8.4^{a,1}	105.0 ± 10.4^{a,1}	90.1 ± 11.1^{3}

[a] The same letters indicate differences that are not significant in the same row ($p \geq 0.05$) and the same numbers indicate differences that are not significant in the same column ($p \geq 0.05$).

The toxicity of quinolones has been reported in several works, and is the reason why the presence of additives, encapsulation agents or complementary molecules are needed to decrease the side effects without losing the antibiotic's therapeutic efficiency.[43] The presence of HMP did not affect the cell viability while no significant differences were found with the untreated control cells ($p \geq 0.05$), suggesting the safety of the biopolymer. It was interesting to observe that the cytotoxicity of Levo at different concentrations was attenuated in the presence of HMP.

The results indicate that, in the presence of HMP, the viability of the cells is not affected at Levo concentrations of up to 100 μg ml^{-1} and a slight cytotoxic effect is observed at 200 μg ml^{-1} with only a 10% reduction in cell viability ($p \leq 0.05$), which is 20% less than that observed with the free drug. These results are very important to potentially validate the application of the BC–HMP system in living organisms (or at least in mammalian cells) as a feasible carrier to reduce the toxic effects associated with the administration of free antibiotics. The reduction of cytotoxicity of Levo when entrapped in the BC–HMP matrix could be associated with the reduction of molecular π-stacking commonly associated with the behavior of free fluoroquinolones in physiological media.[44]

3.5. Efficiency evaluation of HSA incorporation

HSA incorporation in BC–HMP films was evaluated at three different pHs to determine the effect of the residual electric charges of the protein during its entrapment in BC matrices (Table 3). The incorporation of HSA in BC–HMP film was about 10 times higher than that in BC film at pH 5.5, close to the isoionic point of the protein of 5.2. However, HSA incorporation in BC films increased more than 3.5 times at higher pH (*i.e.* 7.0 and 9.0), when the protein was negatively charged. Meanwhile, the entrapment of HSA in BC supplemented with 2.0% HMP showed a higher protein content (around 2.5 mg g^{-1} of matrix) than that found in BC films, independent of the pH ($p \geq 0.05$) (Table 3).

These results suggest that incorporation of HSA is strongly dependent on the film composition because BC is a highly polar matrix. The addition of HMP to BC increased the availability of non-polar groups to the protein due to the high number of hydrophobic patches created by methoxylated galacturonic acid.

Based on the biological properties of HSA which allow it to transport hydrophobic molecules, BC–HMP films were loaded first with HSA and then with Levo. The co-incorporation efficiency for Levo was evaluated with a corresponding comparison with unmodified BC film. The efficiencies of Levo loading into

Table 3 HSA loading in BC and BC–HMP (2.0%) films. The results are expressed as the mean of two independent experiments, each performed in triplicate

	HSA (μg g^{-1} of matrix)	
pH	BC	BC–HMP
5.5	238.7 ± 10.1	2319.8 ± 75.6
7.0	895.9 ± 65.8	2530.3 ± 132.6
9.0	905.6 ± 72.3	2726.7 ± 155.7

BC–HMP and BC were 2.32 ± 0.14 mg g^{-1} and 1.45 ± 0.04 mg g^{-1} respectively when the films were immersed in 5.0 mg ml^{-1} antibiotic solution.

Although a high Levo payload for BC–HMP was observed in presence of HSA. It was found that drug incorporation was reduced almost three times in comparison with the BC–HMP films without HSA. This fact could be explained by HSA binding to the HMP hydrophobic patches in the hybrid matrix, which could reduce the interaction of Levo within the matrix.

3.6. HSA and Levo kinetic release assays

HSA release profiles were analyzed to understand the behavior of the protein once incorporated into the polymeric matrix.

Fig. 9A shows the release curves corresponding to BC and BC–HMP. Interestingly, the similarity between the Levo and HSA release kinetics (see also Fig. 8) suggests a similar kind of interaction within the hybrid BC–HMP matrix. HSA release was delayed after incorporation of HMP into the BC matrix and about 50% of HSA loading remained in the hybrid BC–HMP matrix at the kinetic end-point (Fig. 9A). In contrast, the BC film lost the HSA payload after 6 h. These results suggest that changing the HMP concentration loaded during the synthesis of the BC scaffold could be used to regulate the HSA release kinetic.

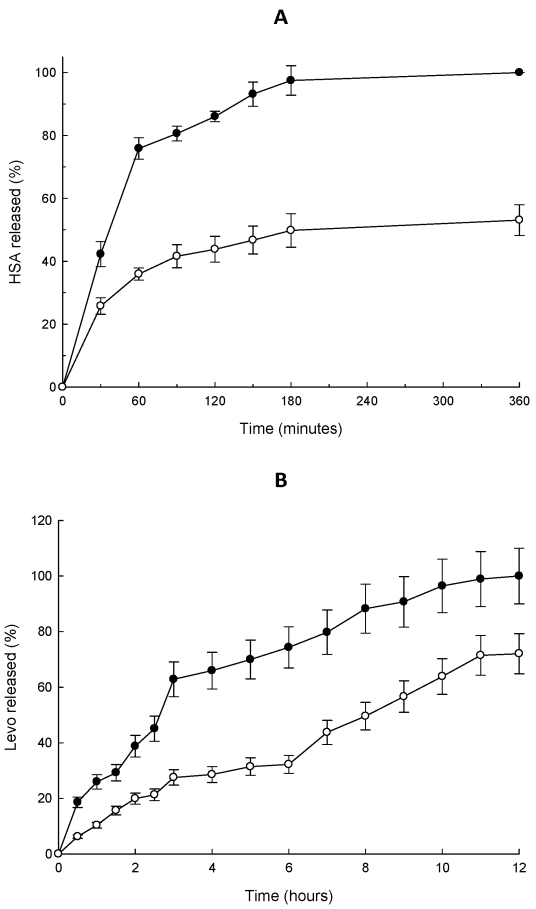

Fig. 9 HSA (A) and Levo (B) release kinetics from BC (– ● –) and BC–HMP (– ○ –) films previously loaded with HSA.

Furthermore, the effect of incorporation of HSA into the polymeric matrices on Levo release was studied (Fig. 8B). In this experiment, all BC films were first dipped into HSA solution before immersion into Levo solution. Although HSA interferes with Levo loading, as mentioned before, it was interesting to observe that the kinetic release profiles of Levo from BC–HSA and BC–HMP–HSA were different to the ones displayed in Fig. 8. There was a decrease in burst release compared to the films without HSA, particularly at the initial time points.

In addition, a decrease in Levo release rate for BC and BC–HMP films was observed. Nevertheless, Levo release percentages were like those observed without the presence of HSA at 6 h incubation. Levo release percentages from BC–HSA and BC–HMP–HSA were 80% and around 40% respectively. Since no plateau in the release curves was observed in either case, the experiment continued for another six hours. During this second period Levo continued to be released from both matrices. Nevertheless, interactions between HSA and Levofloxacin were evidenced by a fluorescence quenching assay (Fig. S4, ESI†).

Results showed a strong dependence of the HSA fluorescence on the presence of Levo. When the drug/protein ratio increased, a drastic decrease of HSA fluorescence intensity was observed. This quenching process clearly reflects HSA–Levo interactions. In a previous study, the interaction of HSA and Levo was determined to have a molecular ratio of 1 : 1, mainly as a result of hydrogen bonding and some van der Waals interactions with HSA sites I and II; the association constant was of the order of 10^4.[45,46] Consequently, changes to the molecular release profiles could be a consequence of these interactions. In conclusion, these results expose another modulating mechanism for Levo release from the hybrid polymeric matrix.

3.7. Antimicrobial studies

The antibacterial activity of BC and BC–HMP films without payload was tested by placing them over the surface of an agar plate containing *S. aureus* (Fig. S6, ESI†). No antibacterial activity could be observed for the unloaded membranes. Next, the antibacterial activity of the incorporated Levo in BC–HMP films was tested against *S. aureus* (Fig. 10A). The results showed that the Levo antimicrobial activity was not inhibited either by the incorporation of the molecule into BC–HMP films or by the

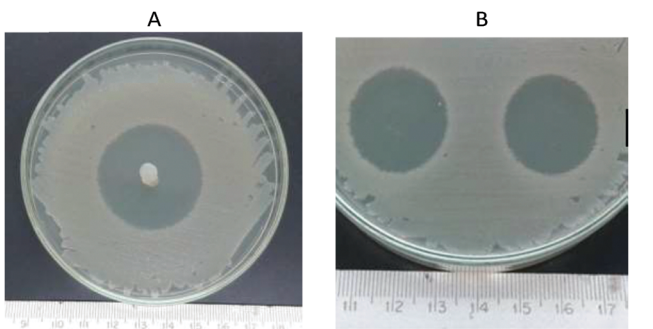

Fig. 10 Antimicrobial activity against *S. aureus* of (A) BC–HMP films loaded with Levo and HSA, (B) control groups: free Levo (right) and Levo + HSA (left).

presence of HSA. This behavior could also be observed in the control groups (Fig. 9B) where Levo and Levo + HSA solutions showed the same inhibitory halos of 22.0 ± 2.0 mm and 23.0 ± 1.5 mm, respectively ($p \geq 0.05$). Moreover, the antimicrobial effect of Levo released from the BC–HMP films resulted in an inhibitory halo of 35.1 ± 4.2 mm, which indicates an improvement of 35% in the antimicrobial activity. This result strongly suggests the possibility of enhanced drug bioavailability caused by entrapment into the BC–HMP polymeric matrix.

4. Conclusions

Addition of HMP to the static cultures of *K. hansenii* produced BC thickening matrices able to efficiently incorporate Levo. SEM images revealed the presence of an interconnected network of BC and HMP biopolymers inside the matrix, making homogeneous and stable gels. TGA and FTIR studies confirmed a collaborative interaction between HMP and BC, suggesting a possible mechanism of pectin integration in the BC network.

Finally, XRD analyses exposed a profound structural change and a strong decrease in crystallinity of the BC network because of the presence of HMP and the associated increased water content. These properties are relevant characteristics since they could improve wound healing and enhance drug diffusion as required in the treatment of dermal infections with patches/films.[40]

Levo and HSA were efficiently incorporated into hybrid cellulose–pectin scaffolds. The Levo and HSA release profiles observed in the BC films in the presence of HMP showed a controlled and sustained molecular delivery over time. The controlled release of both cargo molecules from the scaffold could be associated to the small pores obtained by the inclusion of HMP in the BC matrix. Both ionic and hydrophobic interactions between Levo and HMP were determined by FTIR studies. In addition, the presence of HSA in the hybrid film (caused by simple dipping) modified the profile of Levo release from the scaffold.

Cytotoxicity studies of soluble Levo in mammalian cell cultures showed that it caused a reduction in cell viability in a concentration-dependent manner. However, the Levo cytotoxicity was reduced when HMP and HSA were present in the BC films. The protective effect can be attributed to the interactions of the biopolymer and the protein within the antibiotic, decreasing the level of π-stacking among the drug molecules. Moreover, HMP did not show toxic properties against the tested cells. The main advantages of Levo incorporation into the BC–HMP films containing HSA are the reduction of cytotoxicity in mammalian cells, the controlled release of the antibiotic, and very importantly, the enhanced antimicrobial activity of the antibiotic loaded into BC–HMP membranes against *S. aureus*.

Furthermore, the presence of HSA in the hybrid BC films could allow the transport and controlled release of different molecules useful for wound treatment, like growth factors which are currently failing in therapies because of their high sensitivity to degradation by hydrolases produced by microbial pathogens and present in the tissues around the wounds.

The developed BC–HMP hybrid system containing HSA exhibits new and interesting properties since the stable gels can provide a multipurpose platform for topic application in the delivery of molecules implicated not only in wound healing but also in antimicrobial, oncological or tissue engineering therapies.

Conflicts of interest

The authors declare no conflicts of interest.

Acknowledgements

The present work was supported by Consejo Nacional de Investigaciones Científicas y Técnicas (CONICET, PIP 0498), Universidad Nacional de La Plata (Grants X701 and I159) and Agencia Nacional de Promoción Científica y Técnica (ANPCyT, PICT2011-2116) of Argentina. We wish to thank Mr D. Castrogiovanni, Ms J. Parisi and Mr M. Reigosa (Cell Culture Section, IMBICE) for technical assistance. LCB had a return fellowship from the the Alexander von Humboldt Foundation. Also, we want to thank CPKelco (Buenos Aires, Argentina) for the pectin samples.

References

1 C. K. Sen, G. M. Gordillo, S. Roy, R. Kirsner, L. Lambert, T. K. Hunt, F. Gottrup, G. C. Gurtner and M. T. Longaker, *Wound Repair Regen.*, 2009, **17**, 763–771.
2 C. Lindholm and R. Searle, *Int. Wound J.*, 2016, **13**, 5–15.
3 Y. Lan, W. Li, R. Guo, Y. Zhang, W. Xue and Y. Zhang, *J. Biomater. Sci., Polym. Ed.*, 2014, **25**, 75–87.
4 W. Li, Y. Lan, R. Guo, Y. Zhang, W. Xue and Y. Zhang, *J. Biomater. Appl.*, 2015, **29**, 882–893.
5 R. Guo, Y. Lan, W. Xue, B. Cheng, Y. Zhang, C. Wang and S. Ramakrishna, *J. Tissue Eng. Regener. Med.*, 2017, **11**, 3544–3555.
6 H. Xie, L. Lucchesi, B. Zheng, E. Ladich, T. Pineda, R. Merten, C. Gregory, M. Rutten and K. Gregory, *J. Burn Care Res.*, 2017, **38**, 859–867.
7 Y. N. Martinez, I. Cavello, S. Cavalitto, A. Illanes and G. R. Castro, *Colloids Surf., B*, 2014, **117**, 284–289.
8 J. S. Gonzalez, Y. N. Martínez, G. R. Castro and V. A. Alvarez, *Adv. Mater. Lett.*, 2016, **7**, 640–645.
9 U. Kragh-Hansen, V. T. G. Chuang, M. Otagiri, U. K. R. Ansen, T. Giam and M. O. Tagiri, *Biol. Pharm. Bull.*, 2002, **25**, 695–704.
10 M. T. Larsen, M. Kuhlmann, M. L. Hvam and K. A. Howard, *Mol. Cell. Ther.*, 2016, **4**, 3.
11 Y. Wei, Y. Wang, D. Xia, S. Guo, F. Wang, X. Zhang and Y. Gan, *ACS Appl. Mater. Interfaces*, 2017, **9**, 25138–25151.
12 Z. Liu and X. Chen, *Chem. Soc. Rev.*, 2016, **45**, 1432–1456.
13 J. H. Paton and D. S. Reeves, *Drug Saf.*, 1991, **6**, 8–27.

14 C. Carbon, *Chemotherapy*, 2001, **47**, 9–14.
15 I. Turcu and M. Bogdan, *J. Phys. Chem. B*, 2012, **116**, 6488–6498.
16 M. L. Cacicedo, M. C. Castro, I. Servetas, L. Bosnea, K. Boura, P. Tsafrakidou, A. Dima, A. Terpou, A. Koutinas and G. R. Castro, *Bioresour. Technol.*, 2016, **213**, 172–180.
17 G. F. Picheth, C. L. Pirich, M. R. Sierakowski, M. A. Woehl, C. N. Sakakibara, C. F. de Souza, A. A. Martin, R. da Silva and R. A. de Freitas, *Int. J. Biol. Macromol.*, 2017, **104**, 97–106.
18 M. M. Abeer, M. C. I. Mohd Amin and C. Martin, *J. Pharm. Pharmacol.*, 2014, **66**, 1047–1061.
19 M. L. Cacicedo, I. E. León, J. S. Gonzalez, L. M. Porto, V. A. Alvarez and G. R. Castro, *Colloids Surf., B*, 2016, **140**, 421–429.
20 W. Shao, H. Liu, X. Liu, S. Wang, J. Wu, R. Zhang, H. Min and M. Huang, *Carbohydr. Polym.*, 2015, **132**, 351–358.
21 W. Czaja, A. Krystynowicz, S. Bielecki and R. M. Brown, *Biomaterials*, 2006, **27**, 145–151.
22 H. S. Barud, T. Regiani, R. F. C. Marques, W. R. Lustri, Y. Messaddeq and S. J. L. Ribeiro, *J. Nanomater.*, 2011, **2011**, 721631.
23 F. Munarin, M. C. Tanzi and P. Petrini, *Int. J. Biol. Macromol.*, 2012, **51**, 681–689.
24 G. A. Islan, C. Dini, L. C. Bartel, A. D. Bolzán and G. R. Castro, *Int. J. Pharm.*, 2015, **496**, 953–964.
25 G. A. Islan, V. E. Bosio and G. R. Castro, *Macromol. Biosci.*, 2013, **13**, 1238–1248.
26 J. Weyermann, D. Lochmann and A. Zimmer, *Int. J. Pharm.*, 2005, **288**, 369–376.
27 Y. W. Wang, Q. Wu and G. Q. Chen, *Biomacromolecules*, 2005, **6**, 566–571.
28 D. Lourdin, L. Coignard, H. Bizot and P. Colonna, *Polymer*, 1997, **38**, 5401–5406.
29 M. Kacuráková, *Carbohydr. Polym.*, 2000, **43**, 195–203.
30 J. Lim, J. Yoo, S. Ko and S. Lee, *Food Hydrocolloids*, 2012, **29**, 160–165.
31 J. Gu and J. M. Catchmark, *Carbohydr. Polym.*, 2012, **88**, 547–557.
32 H. C. Huang, L. C. Chen, S. Bin Lin, C. P. Hsu and H. H. Chen, *Bioresour. Technol.*, 2010, **101**, 6084–6091.
33 H. C. Huang, L. C. Chen, S. Bin Lin and H. H. Chen, *Carbohydr. Polym.*, 2011, **83**, 979–987.
34 S. Gunasekaran, K. Rajalakshmi and S. Kumaresan, *Spectrochim. Acta, Part A*, 2013, **112**, 351–363.
35 Y. N. Martinez, L. Pinuel, G. R. Castro and J. D. Breccia, *Appl. Biochem. Biotechnol.*, 2012, **167**, 1421–1429.
36 G. A. Islan, I. P. De Verti, S. G. Marchetti and G. R. Castro, *Appl. Biochem. Biotechnol.*, 2012, **167**, 1408–1420.
37 L. Segal, J. J. Creely, A. E. Martin and C. M. Conrad, *Text. Res. J.*, 1959, **29**, 786–794.
38 Y. Feng, X. Zhang, Y. Shen, K. Yoshino and W. Feng, *Carbohydr. Polym.*, 2012, **87**, 644–649.
39 J. Gu and J. M. Catchmark, *Cellulose*, 2014, **21**, 275–289.
40 Z. Cai and J. Kim, *Cellulose*, 2010, **17**, 83–91.
41 L. Alexandrescu, K. Syverud, A. Gatti and G. Chinga-Carrasco, *Cellulose*, 2013, **20**, 1765–1775.
42 S. Swoboda, K. Oberdorfer, F. Klee, T. Hoppe-Tichy, H. von Baum and H. K. Geiss, *J. Antimicrob. Chemother.*, 2003, **51**, 459–462.
43 Z. L. Bai, Q. Chen, S. D. Yang, F. Zhang, H. Y. Wang, D. L. Yang and W. Y. Ding, *Med. Sci. Monit.*, 2014, **20**, 2205–2212.
44 N. Maurer, K. F. Wong, M. J. Hope and P. R. Cullis, *Biochim. Biophys. Acta, Biomembr.*, 1998, **1374**, 9–20.
45 L. W. Zhang, K. Wang and X. X. Zhang, *Anal. Chim. Acta*, 2007, **603**, 101–110.
46 N. Seedher and P. Agarwal, *J. Lumin.*, 2010, **130**, 1841–1848.